ACS OMEGA

Open Access

http://pubs.acs.org/journal/acsodf

Article

De Novo Designed Cell-Penetrating Peptide Self-Assembly Featuring Distinctive Tertiary Structure

Jaehui Park, Eiki Yamashita, Jaehoon Yu,* Soo Jae Lee,* and Soonsil Hyun*

Cite This: *ACS Omega* 2024, 9, 32991−32999

Read Online

ACCESS | Metrics & More | Article Recommendations | Supporting Information

ABSTRACT: Recent attention has focused on the *de novo* design of proteins, paralleling advancements in biopharmaceuticals. Achieving protein designs with both structure and function poses a significant challenge, particularly considering the importance of quaternary structures, such as oligomers, in protein function. The cell penetration properties of peptides are of particular interest as they involve the penetration of large molecules into cells. We previously suggested a link between the oligomerization propensity of amphipathic peptides and their cell penetration abilities, yet concrete evidence at cellular-relevant concentrations was lacking due to oligomers' instability. In this study, we sought to characterize oligomerization states using various techniques, including X-ray crystallography, acceptor photobleaching Förster resonance energy transfer (FRET), native mass spectrometry (MS), and differential scanning calorimetry (DSC), while exploring the function related to oligomer status. X-ray crystallography revealed the atomic structures of oligomers formed by LK-3, a bis-disulfide bridged dimer with amino acid sequence LKKLCLKLKKLCKLAG, and its derivatives, highlighting the formation of hexamers, specifically the trimer of dimers, which exhibited a stable hydrophobic core. FRET experiments showed that LK-3 oligomer formation was associated with cell penetration. Native MS confirmed higher-order oligomers of LK-3, while an intriguing finding was the enhanced cell-penetrating capability of a 1:1 mixture of L/D-peptide dimers compared to pure enantiomers. DSC analysis supported the notion that this enantiomeric mixture promotes the formation of functional oligomers, crucial for cell penetration. In conclusion, our study provides direct evidence that amphipathic peptide LK-3 forms oligomers at low nanomolar concentrations, underscoring their significance in cell penetration behavior.

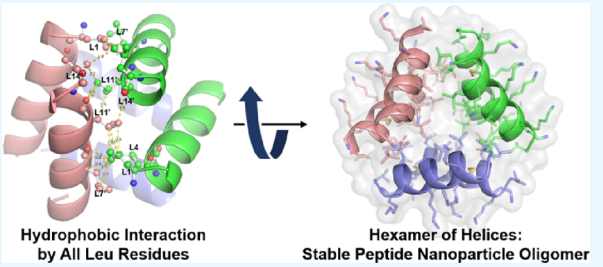

INTRODUCTION

De novo protein design allows for the creation of protein structures that are distinct from those found in nature, assisted with recent development of machine learning.[1] Despite leveraging natural building blocks like coiled-coils,[2] achieving entirely novel topologies remains a significant challenge. Designing functional proteins presents another formidable task. In our recent study, we explore *de novo* designed α-helical amphipathic peptide oligomers, highlighting their potential to enhance cell penetration.[3] However, a notable disparity arises between the peptide concentrations required for cell penetration and those detectable through conventional techniques such as size exclusion chromatography and light scattering experiments.

Recent scholarly attention has been drawn to the question of whether enantiomeric interactions stabilize quaternary structural formations, offering insights into the peptide oligomerization process. Several studies have explored the coassembly of enantiomeric amphipathic peptides into heterochiral rippled β-sheets, demonstrating cooperativity in forming oligomers of racemic mixtures.[4−6] These investigations have highlighted enhancements in viscoelasticity and hydrogelation properties of L/D amphipathic β-hairpin peptides[5] as well as enantioselective recognition between β-sheets.[4] However, conflicting reports[7,8] exist regarding preferences for homochiral and heterochiral β-sheet assembly, including models favoring homochiral tetramer formation[7] and homochiral strand pairing within two intermolecular layers.[8] Despite predictions of heterochiral coiled-coil interactions by Crick,[9] functional investigations into the cooperative interactions of racemates of α-helical oligomers remain scarce.[10] This is notable considering the dominance of interactions between α-helical peptides in functional peptide interactions, especially within membrane polypeptides.

In response, we investigate the oligomer formation of *de novo* designed α-helical amphipathic peptide oligomers at the cellular level corresponding to cell penetration (Figure 1). Initially, X-ray crystallography elucidates the atomic structures of these oligomers, revealing hexameric arrangements comprising a trimer of dimers, with hydrophobic interactions,

Received: April 26, 2024
Revised: July 4, 2024
Accepted: July 9, 2024
Published: July 16, 2024

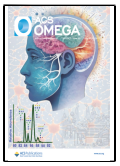

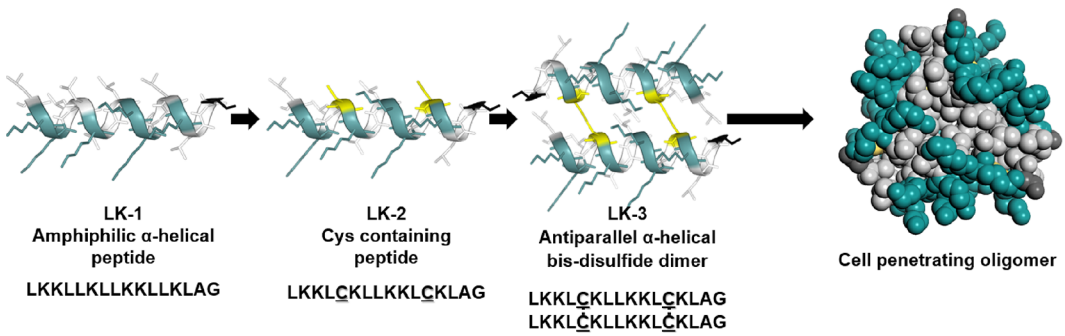

Figure 1. *De novo* designed α-helical amphipathic cell penetrating peptide oligomers. Leu, Lys, and Cys residues are shown in gray, cyan, and yellow, respectively.

particularly involving Leu residues, dictating the novel topology. Subsequently, we validate the existence of stable quaternary structures by detecting oligomer formation using native mass spectrometry and acceptor photobleaching FRET experiments conducted within cellular environments. Furthermore, we observe an intriguing mirror image relationship between the L-form and D-form oligomers. To explore the cell-penetrating potential, we investigated a 1:1 mixture of L-form and D-form LK-3 peptides, noting a remarkable enhancement in cell penetration compared to enantiomerically pure peptides. Additionally, we assess the stability of these quaternary structures using differential scanning calorimetry, revealing a significantly lower melting temperature for the 1:1 mixture of L-form and D-form LK-3 peptides compared to that of their enantiomerically pure counterparts. These findings suggest that cell-penetrating oligomers exhibit minimal structural complexity. Addressing the lack of correlation between heterochiral helix pairings and interactions with the cell membrane, our study reports a homochiral preference in the formation of L- and D-peptide helices oligomers for cell penetration. This enantiomeric interaction preference serves as indirect evidence of functional quaternary structure formation in self-assembling peptides, thus correlating with their cell-penetrating abilities.

MATERIALS AND METHODS

No unexpected or unusually high safety hazards were encountered. Below, we describe the experimental procedures.

Peptide Synthesis. All peptides were synthesized by using the standard fluorenylmethyloxy carbonyl (Fmoc) solid-phase peptide synthesis method on a CEM Liberty Lite microwave peptide synthesizer. All L- and D-amino acids and Oxyma Pure were purchased from Merck. Diisopropylcarbodiimide (DIC), *N*,*N*-diisopropyl ethylamine (DIPEA), and piperidine were purchased from Tokyo Chemical Industry (TCI). Dimethylformamide (DMF) was purchased from Daejung Chemicals & Metals. Synthesis was done on a 0.05 mmol scale on Rink amide MBHA resin (SigmaAldrich). Briefly, the Fmoc protecting group was deprotected using 20% piperidine in DMF. Then, coupling of Fmoc-amino acids to the resins was performed with a mixture of a 5-fold excess of amino acid, 10-folds\ excess of OxymaPure, and 10-fold excess of DIC in DMF. The coupling reaction was assisted with microwave irradiation for 125 s (170 W, 15 s, 75 °C and 30 W, 110 s, 90 °C). Synthesized peptides were detached from the resin by adding a cleavage solution consisting of TFA/H_2O/2,2′-(ethylenedioxy)diethanethiol (DODT, TCI)/triisopropylsilane (TIS, TCI) (94:2.5:2.5:1) for 2 h. This crude peptide mixture was precipitated in 10 mL of a 1:1 solution of ice-cold diethyl ether and *n*-hexane. The peptide suspension was centrifuged (3354*g*, 10 min, 4 °C) and decanted to yield crude peptide. All peptides were purified using semipreparative HPLC (Waters) on a Zorbax C_{18} (3 μm, 4.6 × 150 mm) column as the stationary phase. For the mobile phase, buffer A (water with 0.1% v/v TFA) and buffer B (acetonitrile with 0.1% v/v TFA) were used as a gradient. The Bruker ultrafleXtreme MALDI-TOF mass spectrometer was used to identify peptides.

Cy3 and Cy5 Fluorescence Labeling. Each Cy3 and Cy5 fluorescence was conjugated to the N-terminus of the peptide. For conjugation, Cyanine3 NHS ester (Lumiprobe, 1.2 equiv) or Cyanine5 NHS ester (Lumiprobe, 1.2 equiv) and DIPEA (2.4 equiv) were dissolved in DMF. The N-terminal deprotected resins were reacted with the mixture for 2 h at room temperature.

Oxidative bis-Disulfide Formation (Dimerization). Dimerization reactions of peptides were performed by air oxidation process as previously reported.[11] Briefly, purified C-containing monomeric peptide was dissolved in 0.1 M ammonium bicarbonate, and the mixture was incubated in the atmosphere until the reaction was complete. For fluorescently labeled dimeric peptides, only one fluorescently labeled peptide strand was disulfide bridged with the unlabeled peptide strand. The reaction completion was monitored by HPLC and mass detection. After the reaction, dimeric peptides were purified by HPLC and lyophilized. HPLC traces and mass data are shown in Figure S1.

Crystallization and Structure Determination. All initial crystals were crystallized at a concentration of 50 mg/mL in 20 mM Tris-HCl (pH 7.5) and 100 mM NaCl. LKα14 crystals were grown at 20 °C by using the sitting-drop vapor diffusion method by mixing equal volumes (0.2 + 0.2 μL) of protein and reservoir solution. The reservoir contained 25−27% PEG 3350, 100 mM ammonium phosphate. The crystals belonged to the *P*21 space group, with cell dimensions of a = 35.2, b = 99.7, c = 67.5 Å and diffracted to about 1.92 Å. LK-3 and lk-3 crystals were grown at 20 °C by vapor diffusion method. Crystals were grown from 54 to 60% PEG 400. A variety of crystals have been produced, including hexagonal pyramids, triangles, and rods, but the best resolution was achieved with rod-shaped crystals. LK-3 crystals belonged to the *P*212121 space group, with cell dimensions of a = 34.7, b = 108, and c = 116 Å. lk-3 crystals belonged to the I4122 space group, with cell dimensions of a = b = 64.8 and c = 106 Å. Data sets were collected at the BL44XU beamline at SPring-8, Hyogo, Japan and BL5C, Pohang Light Source, Republic of Korea. Data

https://doi.org/10.1021/acsomega.4c04004
ACS Omega 2024, 9, 32991−32999

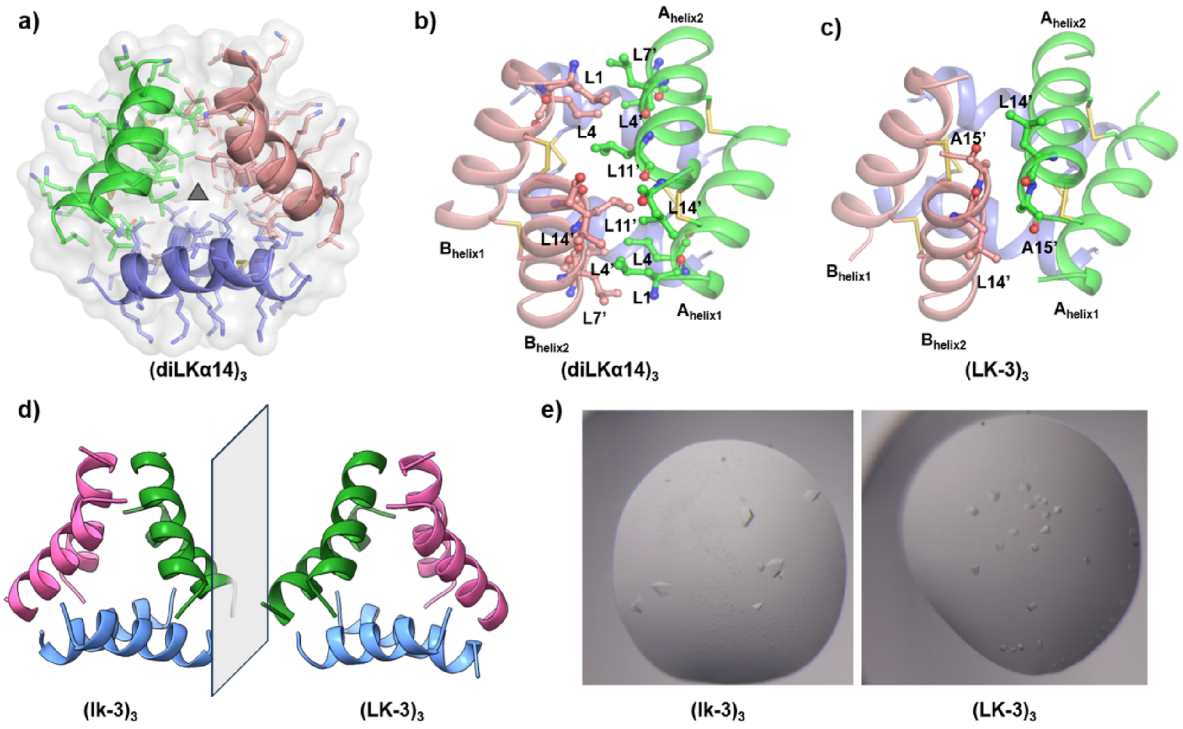

Figure 2. X-ray structures of diLKα14, LK-3, and lk-3. (a) Backbone ribbon structures of trimeric diLKα14, $(diLK\alpha14)_3$. The novel trimeric composed of a trimer of dimer peptides is a perfectly symmetrical trimeric arrangement. (b) Side chain interactions of $(diLK\alpha14)_3$. The intermolecular interactions of chains A and B are shown. The side chains of L1, L4, L7, L11, and L14, which constitute the hydrophobic cavity, are depicted as sticks. (c) $(LK\text{-}3)_3$ overall structure. (d) Mirror-image relationship between $(LK\text{-}3)_3$ and that of $(lk\text{-}3)_3$ is shown. (e) Micrograph of crystals of LK-3 (left) and lk-3 (right).

collection and refinement statistics are listed in Table S1. Structural figures were prepared using PyMOL (http://www.pymol.org). Phasing was performed with the PHENIX program suite. Model building and refinement were achieved using Coot and PHENIX. Data collection statistics are listed in Table S2.

Circular Dichroism (CD). CD spectra were obtained using a Chirascan VX Circular Dichroism detector (Appied Photophysics) with a 0.05 cm path-length cell; CD spectra were scanned from 190 to 260 nm with 0.2 s integration, 1 nm step resolution, and 1 nm bandwidth at 25 °C. Three scans were performed and averaged. Peptide solutions were prepared in 10 mM sodium phosphate (pH 7.4) at a 20 μM concentration.

FRET Assay. Each 100 nM of Cy3 and Cy5-labeled LK-3 were prepared in 96-chimney well plates and incubated in PBS buffer. All samples were prepared on a final 100 μL scale and triplicated. A Spark multimode microplate reader (Tecan Life Sciences) equipped with single monochromators was used. Each sample plate was shaken for 10 s prior to measurements. Samples were excited at 515 or 490 nm, and emission spectra were collected between 560 and 720 nm with a 2 nm step size. Both the excitation and emission slit widths were 20 nm.

Cell Lines and Culture Conditions. HeLa cells (ATCC), the human cervical cancer cell line, were cultured in Dulbecco's modified Eagle's medium (DMEM, HyClone, Thermo Fisher Scientific) containing 10% (v/v) of fetal bovine serum (FBS, HyClone, Thermo Fisher Scientific) and 1% (v/v) of penicillin/streptomycin (Pen−Strep, HyClone, Thermo Fisher Scientific) at 37 °C in the presence of 5% CO_2. Cell viability was determined by means of a colorimetic WST-8 assay. HeLa cells (1×10^4 cells/well) were seeded in a 96-well plate in complete DMEM media. After 24 h of incubation, cultured media were removed, and cells were treated with peptides at various concentrations in fresh complete media. After 12 h incubation, 10 μL of WST-8 reagent (Dojindo Laboratories) was added to each well and incubated for 40 min at 37 °C in a humidified incubator containing 5% CO_2. The absorbance of each well was measured at 450 nm using a 96-well microplate reader (SpectraMax iD3, Molecular Devices).

***In Cellulo* Acceptor Photobleaching FRET Assay.** HeLa cells were seeded in eight-well chambered coverglass (Thermo Fisher Scientific, Thermo Scientific Nunc Lab-Tek Chambered Coverglass) at 2×10^4 cells/well in DMEM containing 10% FBS. After 24 h at 37 °C, the cells were incubated with fluorescence labeled peptides for 1 h and analyzed. An LSM 700 laser scanning confocal fluorescence microscope (Carl Zeiss) equipped with the multiline argon laser (458 nm, 488 nm, 514 nm) was used. To photobleach Cy5, a rectangular region of interest underwent iterations 3 times with the helium neon laser (633 nm, 100% intensity). Fluorescence resonance energy transfer (FRET) efficiency was calculated in a Cy3 present region inside the photobleached region after background correction as $100 \times [(\text{Cy3 postbleach} - \text{Cy3 prebleach})/\text{Cy3 postbleach}]$.

Mass Spectrometry. LC/MS intact mass analysis was performed using a Sciex X500B QTof spectrometer coupled with a Nexera LC System UHPLC instrument (Shimadzu). A 10 μL sample was injected into the LC/MS system for analysis. To capture the complete oligomeric profile of the sample, the column was bypassed and operated in an ESI positive mode. The MS was run in positive ionization mode, and the key parameters were as follows: source temperature, 300 °C; ion spray voltage, 5500 V; pressure of the ion source gases 1−2, 50 psi; declustering potential, 80 V; accumulation time, 0.5 s;

https://doi.org/10.1021/acsomega.4c04004
ACS Omega 2024, 9, 32991−32999

TOF scan range from 100 to 5000 Da with 6 bins to sum. The automated data reconstruction workflow was executed in Sciex OS using Bio Tool Kit software for protein/peptide reconstruction.

Flow Cytometry Analysis. Cell penetration of LK-3, lk-3, and ratio-dependent LK-3 and lk-3 mixture was tested on HeLa cells as previously described.[11] Briefly, HeLa cells (5×10^4 cells/well) were incubated with 5-TAMRA-labeled peptides at various concentrations. After 24 h, cells were collected in microcentrifuge tubes and centrifuged at 18,626 rcf for 2 min and resuspended in 300 μL of PBS. Cellular uptake of peptides was analyzed using a flow cytometer (BD Accuri C6, BD Biosciences). Cellular uptake of peptides was analyzed by flow cytometry analysis and calculated using TAMRA-positive cells (%) and mean fluorescence intensities. Each data point represents mean ± s.d. (n = 4).

Size Exclusion Chromatography. HPLC trances were overlaid using size exclusion column (bio SEC-5, 5 μm, 150 Å, 7.8 × 300 mm column) as a stationary phase at the HPLC (Agilent HPLC 1260 series instrument) system. Sodium phosphate buffer (150 mM, pH 7.4) was used as the mobile phase. The flow rate was 1.0 mL/min. Chromatography data shown in Figure 5b was obtained by injection of 5 nmoles of peptides. A smaller amount of LK-3 up to 0.2 nmol was confirmed to show the same SEC traces. However, the lower concentration of peptides could not be detected due to the molar extinction coefficient.

Differential Scanning Calorimetry. 10 mg/mL LK-3, lk-3, and 1:1 mixture of LK-3 and lk-3 were prepared in 20 mM Tris-HCl (pH 7.5) and 100 mM NaCl. Samples and reference solutions were degassed at 4 °C for 15 min. A buffer solution of 20 mM Tris-HCl (pH 7.5) and 100 mM NaCl was used for the reference cell. Following degassing, the sample and reference were carefully loaded into the cells of a Nano DSC (TA Instruments, New Castle, DE, USA) to avoid the introduction of any air bubbles. The DSC and samples were equilibrated during a brief scan from 25 to 4 °C. Subsequently, scans were performed immediately with a temperature increase from 4 to 110 °C at a rate of 1 °C/min, under a pressure of 3 atm. Samples were then cooled back to 4 °C, and a rescan was performed. Data from the first scan of each sample were used for the analysis.

RESULTS AND DISCUSSION

Homotrimeric Structures of LK-3, lk-3, and diLKα14. In our previous report, we elucidated the molecularity of the oligomer formed by LK-3 through SEC-MALS analysis, identifying it as a tetramer of dimers.[3] However, to gain deeper insight into the atomic level of the oligomer, we attempted to achieve X-ray crystal structures with atomic precision. Remarkably, among the peptides investigated comprising LK-3 and its derivatives, including a truncated LK-3 lacking the Ala-Gly linker (diLKα14)[12] and the enantiomeric D-form of LK-3 (shown as lk-3 in Figure 2) crystals suitable for X-ray crystallography were obtained from three peptides. Surprisingly, only trimeric structures were identified.

Trimers of the α-helical dimer are enigmatic since their structures cannot be explained simply by the arrangement of the α-helices. Our focus shifted to unraveling the intricacies of hydrophobic residue interactions at the atomic level. The X-ray structures revealed 3-fold symmetric arrangements, depicting trimer of dimers structures for LK-3, lk-3, and diLKα14 at resolutions of 2.1, 2.3 and 2.0 Å, respectively (Figure 2, Table S2). To date, only one approach has been identified to form helical tandem repeats that exhibit a spherical shape through C3 symmetry.[13] This is the first report of antiparallel-helical 3-fold symmetric arrangements. Despite the fact that LK-3, lk-3, and diLKα14 peptides crystallized in distinct space groups, the quaternary structures of these three peptides displayed remarkable similarities to those of LK-3. Especially, the diLKα14 sequence was derived from LK-3 by elimination of two C-term residues, Ala-Gly, with the aim of enhancing the interactions in the C-terminal assembly of LK-3 (Figure 2a,b).

The crystal structure with the most pronounced electron density was observed for the diLKα14 oligomer structure. Thus, the subsequent structural description primarily focuses on the diLKα14 oligomer (Figure 2a). A diLKα14 molecule comprises two α-helices forming an antiparallel α-helical dimer, bridged by bis-disulfide bonds (helix1 and helix2). Hydrophobic interactions between Leu residue side chains play a crucial role in the intermolecular interface between the two antiparallel helical bundles. The diLKα14 homotrimer, $(\text{diLK}\alpha14)_3$, takes on a spherical shape with a diameter of 26 Å. It is assembled from three diLKα14 molecules, forming antiparallel dimers of A_{helix1}-A_{helix2}, B_{helix1}-B_{helix2}, and C_{helix1}-C_{helix2}, respectively, through head-to-tail interactions to form a hexamer of trimeric α-helices. Notably, in the diLKα14 oligomeric quaternary structure, no hydrogen bonds or dipole−dipole interactions were detected. Instead, exclusive intermolecular interactions in the diLKα14 oligomeric structure involve hydrophobic interactions between the three pairs of diLKα14 molecules (A-B, B-C, and C-A), with Leu residues playing a crucial role in reinforcing hexamer formation through a hydrophobic interaction network. This assembly creates a hydrophobic cavity (Figure 2b).

Hydrophobic interactions are mainly three groups of networks. The first comprises a network of Leu1 (A), Leu7' (B), and Leu4 (A). The second network includes Leu14' (A), Leu 11' (B), Leu11' (A), Leu1 (B), and Leu7' (A). The third notable interaction occurs between Leu14' (A) and Leu14' (B), resulting in the tight packing of Leu residues at the end of two diLKα14 molecules tightly packed together, forming a hydrophobic vertex with 2-fold symmetry. These interactions are replicated in the three pairs of interactions between A and B chains, between B and C chains, and between C and A chains.

In the crystal structure of $(\text{LK-3})_3$, the oligomeric structure closely resembles that of $(\text{diLK}\alpha14)_3$. However, the electron density in $(\text{LK-3})_3$ appears unclear at several sites, possibly due to the relatively less efficient interactions of the C-term of A_{helix2} and the C-term of B_{helix2} residues compared to $(\text{diLK}\alpha14)_3$ (Figure 2c). In the case of C-term hydrophobic interaction of $(\text{LK-3})_3$, Leu14' (A), Ala15' (A), Leu14' (B), and Ala15' (B) residues contribute to hexamer formation. Additionally, the Ala-Gly linker of LK-3 intervenes in the hydrophobic interaction between Leu14' (A) and Leu14' (B). Furthermore, an attempt was made to obtain the X-ray crystal structure of lk-3, which is composed of D-amino acids. First, the circular dichroism (CD) spectrum of lk-3 was compared with that of LK-3 showing opposite handedness of the enatiomers (Figure S3). The enantiomeric mixture completely suppresses the distinguishing α-helical signal. Interestingly, the X-ray crystal structure of the D-form lk-3 revealed a homotrimer structure, $(\text{lk-3})_3$, which is the exact mirror image of the L-form $(\text{LK-3})_3$ (Figure 2d,e).

https://doi.org/10.1021/acsomega.4c04004
ACS Omega 2024, 9, 32991−32999

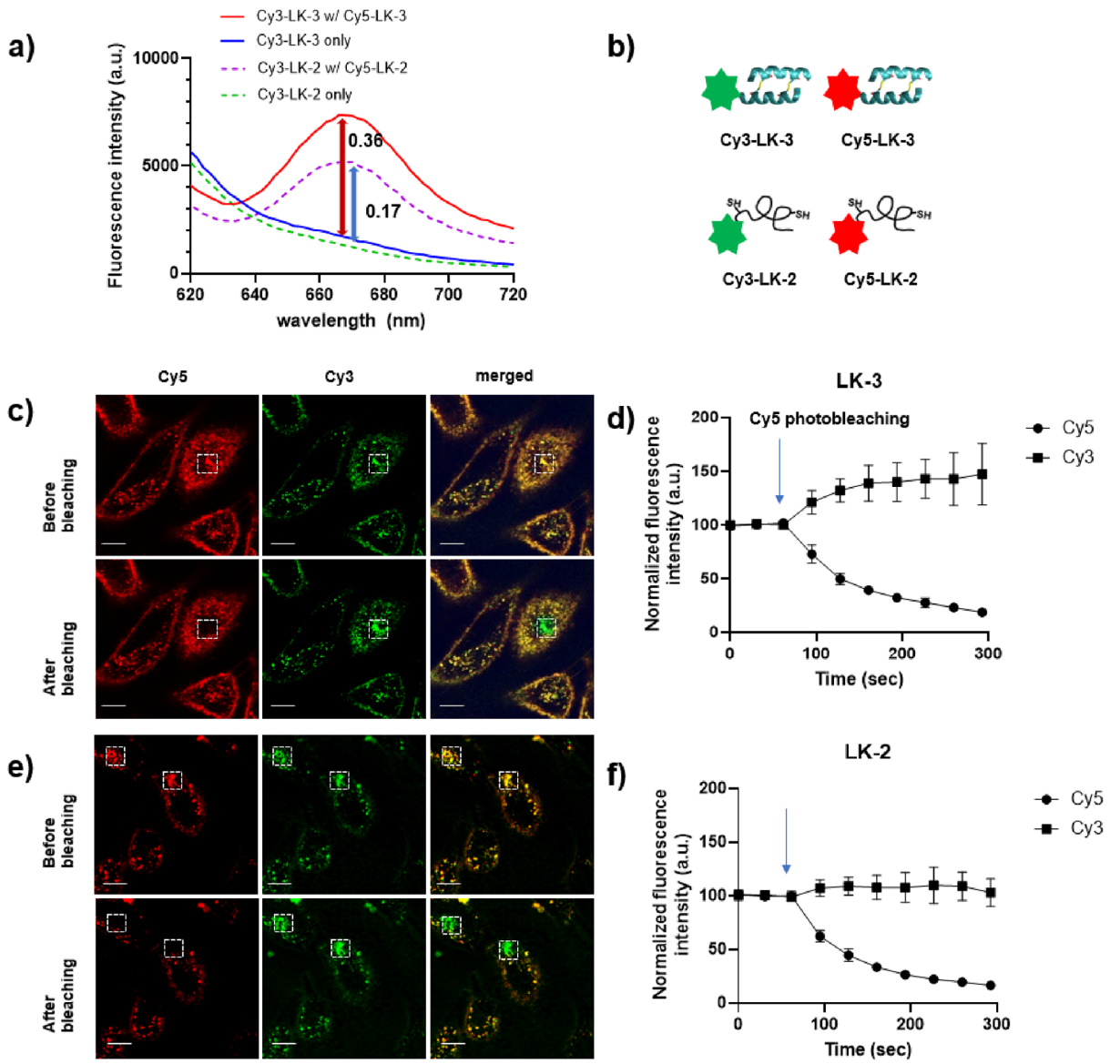

Figure 3. Fluorescence resonance energy transfer (FRET) and acceptor photobleaching FRET analysis of LK-2 and LK-3 labeled with the donor (Cy3) and acceptor (Cy5). (a) Fluorescence emission spectra (620−720 nm) of Cy5 by excitation of Cy3 at 490 nm were recorded for samples containing 100 nM Cy3-labeled LK-3 or LK-2 in phosphate-buffered saline (PBS) solution. Spectra were obtained both in the presence (red line or dotted purple) and absence (blue line or dotted green) of 100 nM Cy5-labeled LK-3 or LK-2, respectively. Each emission scan is presented as the average of three samples (n = 3). (b) Cy3 or Cy5 labeled LK-3 or LK-2 with a cartoon representation. (c) LK-3 showed a specific increase in Cy3 (donor) fluorescence after acceptor (Cy5) bleaching (indicated by the arrow) in a rectangular region of interest. (d) Time-dependent FRET experiments. As donor fluorophore conjugated LK-3 mixed with acceptor fluorophore conjugated LK-3. The positive control consisted of 100 nM Cy3-LK-3 and Cy5-LK-3 (1:1 mixture) (FRET efficiency 47 ± 29%). (e) No changes in the Cy3 signal intensity were observed in LK-2 after bleaching of Cy5. (f) Time-dependent FRET experiments. Donor fluorophore conjugated LK-2 and mixed with acceptor fluorophore LK-2 served as negative control in FRET measurements (FRET efficiency: 2.9 ± 13.8%). Scale bars: 10 μm. (mean ± s.d., n = 3 cells). Experimental details are shown in Materials and Methods.

Large FRET Signals of the Donor Cy3 and Acceptor Cy5 Labeled bis-Disulfide Dimer Peptide Pair, Cy3-LK-3, and Cy5-LK-3 Show Oligomerization at Nanomolar Concentrations. The Förster resonance energy transfer (FRET) assay is commonly applied to study the protein assembly.[14] In our study, we conducted a FRET experiment to directly assess the oligomerization of LK-3 at nanomolar concentrations. Specifically, we compared the FRET efficiency of a bis-disulfide dimer LK-3 labeled with two different fluorescence pair (Cy3 and Cy5, Figure S1) with that of a monomer LK-2 labeled with the same fluorescence pair. This comparison was based on the anticipation that structurally well-organized assemblies should exhibit a more robust FRET signal compared with random interactions of fluorescence pairs. Upon incubating 100 nM Cy3-LK-3 with an equivalent concentration of Cy5-LK-3, we observed an increased Cy5-LK3 FRET signal upon excitation in the donor fluorescence (Cy3). The FRET efficiencies of LK-3 and the monomer, LK-2, were calculated as 0.36 and 0.17, respectively (Figure 3a). Consequently, we found that the FRET signal of each fluorescently labeled monomer LK-2 was weaker than that of LK-3.

***In Cellulo* Oligomerization by Acceptor Photobleaching FRET.** Solution FRET experiments offer valuable insights

https://doi.org/10.1021/acsomega.4c04004
ACS Omega 2024, 9, 32991−32999

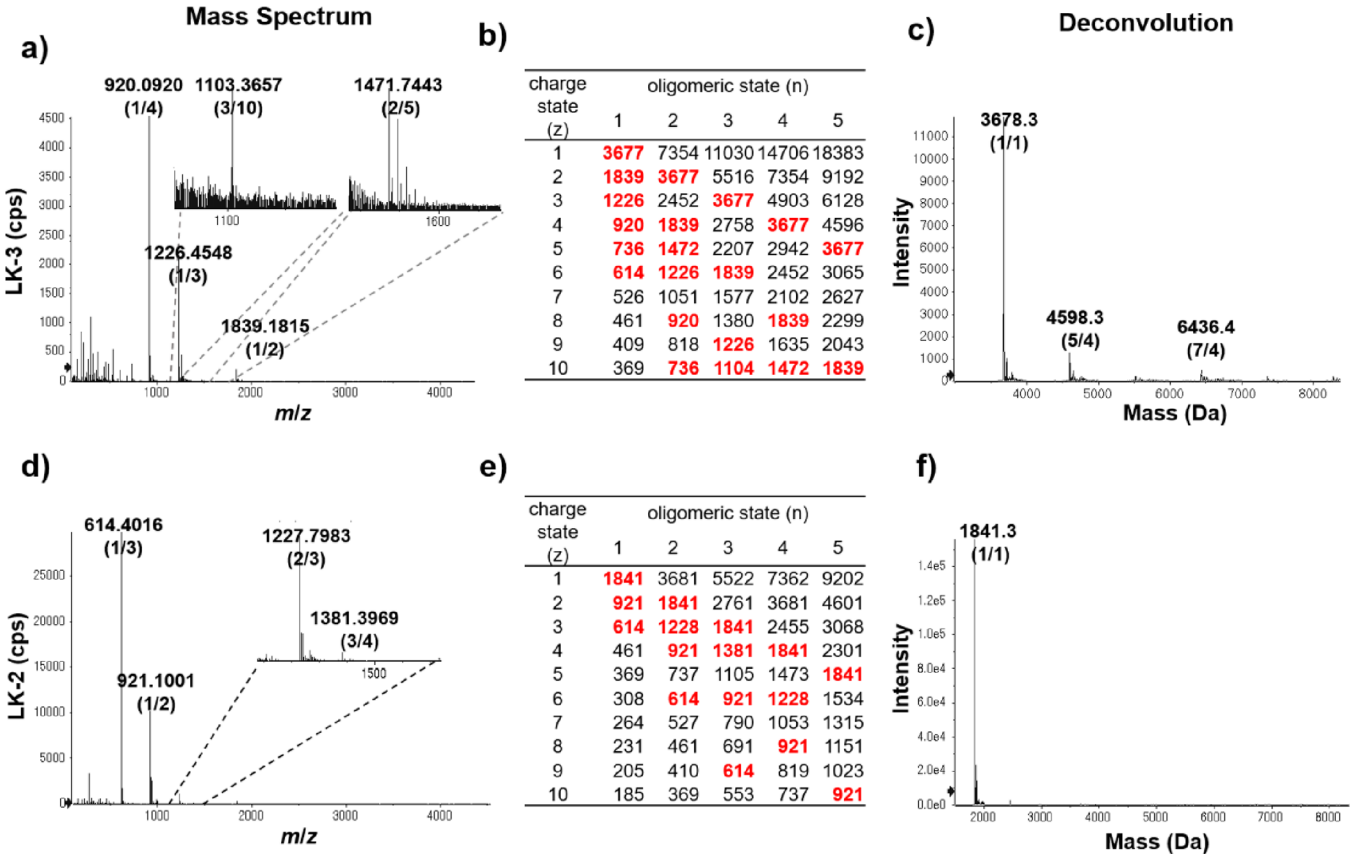

charge state (z)	oligomeric state (n) 1	2	3	4	5
1	**3677**	7354	11030	14706	18383
2	**1839**	**3677**	5516	7354	9192
3	**1226**	2452	**3677**	4903	6128
4	**920**	**1839**	2758	**3677**	4596
5	**736**	**1472**	2207	2942	**3677**
6	**614**	**1226**	**1839**	2452	3065
7	526	1051	1577	2102	2627
8	461	**920**	1380	**1839**	2299
9	409	818	**1226**	1635	2043
10	369	**736**	**1104**	**1472**	**1839**

charge state (z)	oligomeric state (n) 1	2	3	4	5
1	**1841**	3681	5522	7362	9202
2	**921**	**1841**	2761	3681	4601
3	**614**	**1228**	**1841**	2455	3068
4	461	**921**	**1381**	**1841**	2301
5	369	737	1105	1473	**1841**
6	308	**614**	**921**	**1228**	1534
7	264	527	790	1053	1315
8	231	461	691	**921**	1151
9	205	410	**614**	819	1023
10	185	369	553	737	**921**

Figure 4. Mass spectrum of LK-3 and LK-2 in 50 mM ammonium acetate (pH 6.9) under native conditions. (a) TOF-MS of LK-3. Insets provide detailed views of the expected regions for larger oligomers. The notation in parentheses denotes the oligomeric state divided by the charge state (n/z). For instance, 2/4 encompasses dimer (+4), trimer (+6), and tetramer (+8) components, highlighting the diverse constituents within this fraction. Peptide signals corresponding to the higher oligomeric states can be seen around m/z 1100 and 1450, featuring distinctive peaks for trimeric and dimeric states (3/10 and 2/5, respectively). (b) Oligomer peaks formed by LK-3 in (a) were assigned by comparing the experimentally determined n/z values with theoretical calculations. Experimentally observed states are highlighted in red. (c) Representative deconvoluted mass spectrum (Input m/z: 500.0 to 1000.0 Da, spectrum isotope resolution: Resolved (30000)) of intact LK-3. The automated data reconstruction workflow was executed in Sciex OS Software using the Bio Tool Kit for protein/peptide reconstruction. (d) TOF-MS of LK-2. Inset provides a detailed view of the expected regions for larger oligomers. Peptide signals corresponding to the higher oligomeric states can be seen around m/z 1228 and 1381, featuring distinctive peaks for dimeric and trimeric states (2/3 and 3/4, respectively). (e) Oligomer peaks formed by LK-2 in (d). Experimentally observed states are highlighted in red. (f) Representative deconvoluted mass spectrum (Input m/z: 500.0 to 1000.0 Da, spectrum isotope resolution: Resolved (30000)) of intact LK-2.

into peptide intermolecular interactions. However, a significant drawback of this method is its inability to provide conclusive evidence that LK-3 oligomerizes under cellular conditions. In order to investigate oligomerization in living cells, we employed confocal fluorescence microscopy analysis of FRET between peptides labeled with two different fluorescent dye pairs, a potent tool in this context.[15] FRET can be detected only when the distance between two fluorescent peptides is less than 10 nm. Thus, we chose *in cellulo* microscopic acceptor photobleaching FRET experiment for studying LK-3 oligomerization, given that oligomerization occurs at similar spatial scales.

The results indicate that photobleaching the acceptor fluorescence Cy5 enhances the fluorescence intensity of donor Cy3 upon incubation with a 1:1 mixture of Cy3-LK-3 and Cy5-LK-3 (Figure 3c,d). The calculated FRET efficiency for LK-3 was *ca.* 25%. In contrast, the results of the same experiment using a 1:1 mixture of Cy3-LK-2 and Cy5-LK-2 showed no significant change in donor fluorescence intensity (Figure 3e,f). Consequently, these findings support the conclusion that covalently disulfide-bonded dimeric LK-3 forms relatively stable oligomers, while monomeric LK-2 does not form stable oligomers under the experimental conditions employed for cellular FRET analysis.

Native Mass Spectrometry Reveals the Formation of Oligomers in a Buffer Solution. Next, we conducted a native mass spectrometry (MS) experiment to investigate the oligomeric state of LK-3[16] in a buffer condition. The experiment was carried out using a solution of LK-3 in ammonium acetate, a useful additive for native ESI-MS.[17] The oligomeric states in aqueous solutions were observed within the time frame of the MS analysis. Direct analysis of the bis-disulfide bridged dimer LK-3 yielded a mass spectrum with major peaks at 1226.4548 (1/3) and 920.0920 (1/4) Da, corresponding to mass divided by charge (n/z value). Additionally, less intense signals corresponding to oligomers were detected, as shown in the inset spectrum (Figure 4a) and compared with the oligomeric n-z values with theoretical calculations (Figure 4b). The reconstructed MS chromatogram, generated through data analysis software, displayed signals of these oligomers alongside LK-3 (Figure 4c).

https://doi.org/10.1021/acsomega.4c04004
ACS Omega 2024, 9, 32991−32999

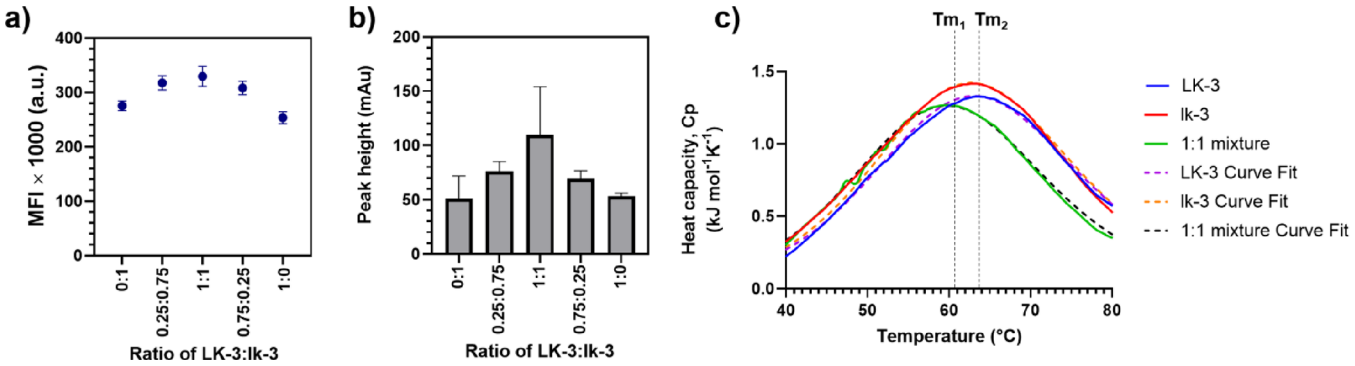

Figure 5. Enantiomeric interaction and cell penetration. (a) Cell penetration and (b) intensity of the oligomer in size exclusion chromatography of a ratio-dependent mixture of LK-3 and lk-3. Data are presented as mean ± s.d. (n = 4). (c) Temperature stability of LK-3, lk-3, and 1:1 mixture of LK-3 and lk-3 as measured by DSC. Two melting events are indicated by Tm_1 and Tm_2.

However, two free Cys containing reduced monomeric LK-2 was detected by MS as predominantly monomers (Figure 4d) and compared with the theoretical values (Figure 4e). Therefore, no significant reconstructed peaks corresponding to oligomeric states of monomer LK-2 were observed by native mass spectrometry (Figure 4f). The employed reconstructed MS method for native MS screening provides immediate and valuable insights into the structural states of larger oligomers, facilitating their precise identification as previously elucidated.[18]

Enantiomeric Interactions of the L and D-form of LK-3, Cell Penetration, and Oligomeric Properties. Recently, significant attention has been directed toward determining whether the enantiomeric interaction stabilizes the quaternary structural formation. We propose that these cooperative interactions offer insights into not only the formation of stable peptide oligomers but also the functional oligomeric units. In our study, we explored the cooperative function between L- and D-peptide helices in the context for their cell penetration. This enantiomeric interaction serves as direct evidence of oligomeric quaternary structure formation in self-assembling peptides, thereby offering insights into their cell-penetrating abilities.

Based on the observation that LK-3 forms a stable oligomer conferring cell penetrating propensity and the mirror image relationship of $(LK\text{-}3)_3$ and $(lk\text{-}3)_3$, we aimed to investigate the impact of the enantiomeric interaction between the L- and D-form of LK-3. To do this, we examined the cell penetrating abilities of enantiomeric mixtures at varying ratios by mixing the L- and D-form enantiomers of LK-3. Interestingly, compared to the enantiomerically pure L or D forms, the 1:1 mixture of L and D form LK-3 showed a *ca.* 30% increase in cell permeability (Figure 5a). Next, we explored the oligomeric tendencies of LK-3 using size exclusion gel chromatography. The analysis revealed a 2-fold increase in the intensity of peak corresponding to the oligomeric nanoparticle, when subjecting an equimolar mixture of L and D-form LK-3 to analysis (Figure 5b). The intensities of the oligomer were further analyzed in relation to the ratios of the L and D-form LK-3 mixtures. The results show that the propensity to form oligomers via enantiomeric interactions is positively correlated with the cell-penetrating abilities of the mixtures, underscoring the promotion of cell penetration ability through enhanced oligomer formation tendency.

In our efforts to elucidate the enhancement of cell-penetrating ability of the enantiomeric mixture of LK-3, we attempted to crystallize and solve the X-ray crystal structure of the enantiomeric mixture multiple times, aiming to gain atomic-level insights into the racemic mixture and ascertain if there was an increase in the number of interpeptide contacts. However, our endeavors were met with difficulty, as we could only obtain enantiomerically pure crystals instead of heterochiral oligomers (Figure S2).

Finally, differential scanning calorimetry (DSC) was performed to monitor the melting temperatures of the oligomers of LK-3, that of lk-3, and the 1:1 mixture of LK-3 and lk-3 (Figure 5c). The results revealed that the melting temperatures of LK-3 and lk-3 were measured as 63.8 and 63.5 °C (both indicated by T_{m2}), respectively, which did not show significant differences. However, the temperature shift induced by the 1:1 mixture was measured as 60.5 °C (indicated by T_{m1}). This result showed that enantiomerically pure peptides tend to form the higher-order oligomers compared to the 1:1 mixture, resulting in higher T_m values.

Based on SEC and DSC data, the improvement in cell-penetrating ability observed in a 1:1 mixture of the L and D-form of LK-3 is attributed to an increased tendency to form functional oligomers. The T_m of the relevant oligomer was found to be 60.5 °C. Additionally, the lack of discovery of new types of interactions and the relatively low T_m of the 1:1 mixture indicate that the formation of completely new heterochiral oligomers does not occur.

CONCLUSIONS

In conclusion, the amphipathic cell-penetrating peptide, LK-3, forms nanosized oligomers that have been suggested as a determinant for cell penetration. Structural investigation using X-ray determination reveals that hydrophobic interactions between Leu residues in dimeric bundle peptides create a hydrophobic cavity formed by the assembly of three dimeric helices inside the hexamer. *In cellulo* FRET experiments verify the formation of LK-3 oligomers at nanomolar concentrations in cells. Native mass analysis confirms that LK-3 prefers to form oligomers and shows the potential for higher levels of oligomer formation.

Based on the discovery of the enantiomeric relationship between the oligomeric structures $(LK\text{-}3)_3$ and $(lk\text{-}3)_3$, we hypothesized that functional enhancement conditions provide information about the minimal unit of cell-penetrating function. In particular, the racemic mixture of LK-3 and lk-3 shows an approximately 30% increase in cell penetration compared to each enantiomerically pure peptide, correlating

https://doi.org/10.1021/acsomega.4c04004
ACS Omega 2024, 9, 32991−32999

with the oligomer formation tendency measured by SEC. However, attempts to obtain X-ray crystals of newly formed heterochiral oligomers were unsuccessful. The thermal stability of each oligomer and the 1:1 mixture was determined, resulting in a lower melting temperature for the 1:1 mixture.

Therefore, the enantiomerically pure peptides LK-3 and lk-3 tended to form higher-order oligomers, as judged by the native MS and DSC data, but the functional cell-penetrating oligomers were interpreted as oligomers showing a T_m of 60.5 °C. Finally, we obtained atomic-level structural information for peptide nanoparticles composed of antiparallel α-helices, providing insight into the design of functional supramolecular protein assemblies. These findings pave the way for adopting successful designs of novel motifs to form oligomers into functional and structural peptide assemblies.

■ ASSOCIATED CONTENT

Supporting Information

The Supporting Information is available free of charge at https://pubs.acs.org/doi/10.1021/acsomega.4c04004.

Chromatograms of synthesized peptides, micrograph of crystals of 1:1 mixture of LK-3 and lk-3, and X-ray crystallography statistics for data-collection, phasing, and refinement (PDF)

■ AUTHOR INFORMATION

Corresponding Authors

Jaehoon Yu − *Department of Chemistry & Education, Seoul National University, Seoul 08826, Korea; CAMP Therapeutics Co., Ltd., Seoul 08826, Korea;* orcid.org/0000-0003-4222-4398; Email: jhoonyu@snu.ac.kr

Soo Jae Lee − *College of Pharmacy, Chungbuk National University, Cheongju 28160, Korea*; Email: sjlee@chungbuk.ac.kr

Soonsil Hyun − *College of Pharmacy, Chungbuk National University, Cheongju 28160, Korea;* orcid.org/0000-0002-3400-7353; Email: shyun@chungbuk.ac.kr

Authors

Jaehui Park − *College of Pharmacy, Chungbuk National University, Cheongju 28160, Korea*

Eiki Yamashita − *Institute for Protein Research, Osaka University, Osaka 565-0871, Japan*

Complete contact information is available at: https://pubs.acs.org/10.1021/acsomega.4c04004

Author Contributions

The manuscript was written through contributions of all authors. S.H., J.Y., and S.J.L. conceived of the presented idea. J.P. and S.H. carried out the experiments. S.H., J.Y., and S.J.L. supervised the findings of this work. J.P. and E.Y. performed X-ray crystallization experiments. All authors discussed the results and contributed to the final manuscript. S.H., J.P., and S.J.L. wrote the manuscript. All authors have given approval to the final version of the manuscript.

Notes

The authors declare no competing financial interest.

■ ACKNOWLEDGMENTS

This work was financially supported by a grant (NRF-2021R1I1A1A01059834 and MRC 2017R1A5A2015541) from NRF of Korea and by "Regional Innovation Strategy (RIS)" through the National Research Foundation of Korea (NRF) funded by the Ministry of Education (MOE) (2021RIS-001).

■ ABBREVIATIONS

MS;mass spectrometry; DSC;differential scanning calorimetry; FRET;Förster resonance energy transfer; Fmoc;fluorenylmethyloxy carbonyl; DIC;diisopropylcarbodiimide; DIPEA;*N*,*N*-diisopropyl ethylamine; DMF;dimethylformamide; DODT;2,2′-(Ethylenedioxy)diethanethiol; TIS;triisopropylsilane; MALDI-TOF;matrix-assisted laser desorption/ionization-time-of-flight

■ REFERENCES

(1) Kuhlman, B.; Dantas, G.; Ireton, G. C.; Varani, G.; Stoddard, B. L.; Baker, D. Design of a Novel Globular Protein Fold with Atomic-Level Accuracy. *Science* **2003**, *302* (5649), 1364−1368.

(2) Satler, T.; Hadži, S.; Jerala, R. Crystal Structure of de Novo Designed Coiled-Coil Protein Origami Triangle. *J. Am. Chem. Soc.* **2023**, *145* (31), 16995−17000.

(3) Hyun, S.; Lee, Y.; Jin, S. M.; Cho, J.; Park, J.; Hyeon, C.; Kim, K. S.; Lee, Y.; Yu, J. Oligomer Formation Propensities of Dimeric Bundle Peptides Correlate with Cell Penetration Abilities. *ACS Cent. Sci.* **2018**, *4* (7), 885−893.

(4) Chung, D. M.; Nowick, J. S. Enantioselective molecular recognition between beta-sheets. *J. Am. Chem. Soc.* **2004**, *126* (10), 3062−3063. From NLM Medline. Dutta, S.; Foley, A. R.; Warner, C. J. A.; Zhang, X.; Rolandi, M.; Abrams, B.; Raskatov, J. A. Suppression of Oligomer Formation and Formation of Non-Toxic Fibrils upon Addition of Mirror-Image Abeta42 to the Natural l-Enantiomer. *Angew. Chem.* **2017**, *56* (38), 11506−11510.

(5) Nagy, K. J.; Giano, M. C.; Jin, A.; Pochan, D. J.; Schneider, J. P. Enhanced mechanical rigidity of hydrogels formed from enantiomeric peptide assemblies. *J. Am. Chem. Soc.* **2011**, *133* (38), 14975−14977. Nagy-Smith, K.; Beltramo, P. J.; Moore, E.; Tycko, R.; Furst, E. M.; Schneider, J. P. Molecular, Local, and Network-Level Basis for the Enhanced Stiffness of Hydrogel Networks Formed from Coassembled Racemic Peptides: Predictions from Pauling and Corey. *ACS Cent Sci.* **2017**, *3* (6), 586−597.

(6) van Groen, T.; Schemmert, S.; Brener, O.; Gremer, L.; Ziehm, T.; Tusche, M.; Nagel-Steger, L.; Kadish, I.; Schartmann, E.; Elfgen, A.; et al. The Abeta oligomer eliminating D-enantiomeric peptide RD2 improves cognition without changing plaque pathology. *Sci. Rep* **2017**, *7* (1), 16275. From NLM Medline.

(7) Li, X.; Rios, S. E.; Nowick, J. S. Enantiomeric β-sheet peptides from Aβ form homochiral pleated β-sheets rather than heterochiral rippled β-sheets. *Chem. Sci.* **2022**, *13* (26), 7739−7746.

(8) Liu, X.; Gellman, S. H. Comparisons of β-Hairpin Propensity Among Peptides with Homochiral or Heterochiral Strands. *ChemBioChem.* **2021**, *22* (18), 2772−2776.

(9) Crick, F. The packing of [alpha]-helices: simple coiled-coils. *Acta Crystallogr.* **1953**, *6* (8−9), 689−697.

(10) Kreitler, D. F.; Yao, Z.; Steinkruger, J. D.; Mortenson, D. E.; Huang, L.; Mittal, R.; Travis, B. R.; Forest, K. T.; Gellman, S. H. A Hendecad Motif Is Preferred for Heterochiral Coiled-Coil Formation. *J. Am. Chem. Soc.* **2019**, *141* (4), 1583−1592.

(11) Hyun, S.; Kim, D.; Cho, J.; Jeong, D.; Chung, D. H.; Yu, J. Design and Optimization of an α-Helical Bundle Dimer Cell-Penetrating Peptide for In Vivo Drug Delivery. *Bioconjugate Chem.* **2022**, *33* (12), 2420−2427.

(12) Dalgicdir, C.; Sayar, M. Conformation and Aggregation of LKα14 Peptide in Bulk Water and at the Air/Water Interface. *J. Phys. Chem. B* **2015**, *119* (49), 15164−15175.

(13) Doyle, L. A.; Takushi, B.; Kibler, R. D.; Milles, L. F.; Orozco, C. T.; Jones, J. D.; Jackson, S. E.; Stoddard, B. L.; Bradley, P. De novo design of knotted tandem repeat proteins. *Nat. Commun.* **2023**, *14* (1), 6746.

(14) Sreenivasan, R.; Heitkamp, S.; Chhabra, M.; Saecker, R.; Lingeman, E.; Poulos, M.; McCaslin, D.; Capp, M. W.; Artsimovitch, I.; Record, M. T., Jr. Fluorescence Resonance Energy Transfer Characterization of DNA Wrapping in Closed and Open Escherichia coli RNA Polymerase-lambdaP(R) Promoter Complexes. *Biochemistry* **2016**, *55* (14), 2174−2186.
(15) Eckenstaler, R.; Benndorf, R. A. A Combined Acceptor Photobleaching and Donor Fluorescence Lifetime Imaging Microscopy Approach to Analyze Multi-Protein Interactions in Living Cells. *Front Mol. Biosci* **2021**, *8*, No. 635548. Methods.
(16) Liu, C.; Henning-Knechtel, A.; Österlund, N.; Wu, J.; Wang, G.; Gräslund, R. A. O.; Kirmizialtin, S.; Luo, J. Oligomer Dynamics of LL-37 Truncated Fragments Probed by α-Hemolysin Pore and Molecular Simulations. *Small* **2023**, *19* (37), No. 2206232. Wu, J.; Österlund, N.; Wang, H.; Sternke-Hoffmann, R.; Pupart, H.; Ilag, L. L.; Gräslund, A.; Luo, J. Identifying the role of co-aggregation of Alzheimer's amyloid-β with amorphous protein aggregates of non-amyloid proteins. *Cell Rep. Phys. Sci.* **2022**, *3* (9), No. 101028. Österlund, N.; Moons, R.; Ilag, L. L.; Sobott, F.; Gräslund, A. Native Ion Mobility-Mass Spectrometry Reveals the Formation of β-Barrel Shaped Amyloid-β Hexamers in a Membrane-Mimicking Environment. *J. Am. Chem. Soc.* **2019**, *141* (26), 10440−10450.
(17) Konermann, L. Addressing a Common Misconception: Ammonium Acetate as Neutral pH "Buffer" for Native Electrospray Mass Spectrometry. *J. Am. Soc. Mass Spectrom.* **2017**, *28* (9), 1827−1835.
(18) Lu, Y.; Liu, H.; Saer, R. G.; Zhang, H.; Meyer, C. M.; Li, V. L.; Shi, L.; King, J. D.; Gross, M. L.; Blankenship, R. E. Native Mass Spectrometry Analysis of Oligomerization States of Fluorescence Recovery Protein and Orange Carotenoid Protein: Two Proteins Involved in the Cyanobacterial Photoprotection Cycle. *Biochemistry* **2017**, *56* (1), 160−166. Bern, M.; Caval, T.; Kil, Y. J.; Tang, W.; Becker, C.; Carlson, E.; Kletter, D.; Sen, K. I.; Galy, N.; Hagemans, D.; et al. Parsimonious Charge Deconvolution for Native Mass Spectrometry. *J. Proteome Res.* **2018**, *17* (3), 1216−1226.

https://doi.org/10.1021/acsomega.4c04004
ACS Omega 2024, 9, 32991−32999